

# The N-terminal Domain of the *Drosophila* Mitochondrial Replicative DNA Helicase Contains an Iron-Sulfur Cluster and Binds DNA\*

Received for publication, June 7, 2014, and in revised form, July 2, 2014. Published, JBC Papers in Press, July 14, 2014, DOI 10.1074/jbc.M114.587774

Johnny Stiban<sup>†§1</sup>, Gregory A. Farnum<sup>‡</sup>, Stacy L. Hovde<sup>‡</sup>, and Laurie S. Kaguni<sup>†‡2</sup>

From the <sup>†</sup>Department of Biochemistry and Molecular Biology, and Center for Mitochondrial Science and Medicine, Michigan State University, East Lansing, Michigan 48824 and the <sup>‡</sup>Department of Biology and Biochemistry, Birzeit University, P. O. Box 14, West Bank 627, Palestine

**Background:** Despite high evolutionary conservation, the function of the N-terminal domain (NTD) of mtDNA helicase remains elusive.

**Results:** *Drosophila* NTD contains an iron-sulfur cluster and binds DNA.

**Conclusion:** The iron-sulfur cluster in mtDNA helicase enhances protein stability, and may regulate its biological functions.

**Significance:** Discovery of an Fe-S cluster in insect mtDNA helicase presents a novel opportunity to explore species-specific relationships in the replisome.

The metazoan mitochondrial DNA helicase is an integral part of the minimal mitochondrial replisome. It exhibits strong sequence homology with the bacteriophage T7 gene 4 protein primase-helicase (T7 gp4). Both proteins contain distinct N- and C-terminal domains separated by a flexible linker. The C-terminal domain catalyzes its characteristic DNA-dependent NTPase activity, and can unwind duplex DNA substrates independently of the N-terminal domain. Whereas the N-terminal domain in T7 gp4 contains a DNA primase activity, this function is lost in metazoan mtDNA helicase. Thus, although the functions of the C-terminal domain and the linker are partially understood, the role of the N-terminal region in the metazoan replicative mtDNA helicase remains elusive. Here, we show that the N-terminal domain of *Drosophila melanogaster* mtDNA helicase coordinates iron in a 2Fe-2S cluster that enhances protein stability *in vitro*. The N-terminal domain binds the cluster through conserved cysteine residues (Cys<sup>68</sup>, Cys<sup>71</sup>, Cys<sup>102</sup>, and Cys<sup>105</sup>) that are responsible for coordinating zinc in T7 gp4. Moreover, we show that the N-terminal domain binds both single- and double-stranded DNA oligomers, with an apparent  $K_d$  of ~120 nM. These findings suggest a possible role for the N-terminal domain of metazoan mtDNA helicase in recruiting and binding DNA at the replication fork.

Mitochondrial DNA plays an essential role in the life and death of cells. The circular mtDNA molecule in animals contains 37 genes, including 13 that encode polypeptide components essential for oxidative phosphorylation (1, 2). The depletion of mtDNA resulting from defects in either nucleotide metabolism or mtDNA replication can lead to multiple adverse

effects in humans (3, 4). Replication of mtDNA is mediated by the replisome, a dynamic multiprotein-mtDNA complex that coordinates DNA unwinding and duplication. In metazoans, the minimal mitochondrial replisome consists of DNA polymerase  $\gamma$  (comprising a catalytic core, PolyA, and an accessory subunit, PolyB), mtDNA helicase, and single-stranded DNA-binding protein (5). As for many replicative DNA helicases, mtDNA helicase catalyzes the NTP-dependent unwinding of DNA at the mitochondrial replication fork in the 5' to 3' direction (6). In humans, the replicative mtDNA helicase (TWINKLE) is integral to the well being of the organism, as mutations affecting the gene that encodes it (*PEO1*) have been reported in patients with adult onset autosomal dominant progressive external ophthalmoplegia, as well as in compound heterozygous patients with more severe mitochondrial pathologies such as infantile onset spinocerebellar ataxia and hepatocerebral mtDNA depletion syndromes (3, 7, 8). Indeed, mtDNA helicase is essential for mtDNA maintenance; the expression of helicase variants causes mtDNA deletion and depletion in various tissues and cell lines (7, 9–13).

The mtDNA helicase exhibits strong amino acid sequence homology with bacteriophage T7 gene 4 protein primase-helicase (7, 14). Based on biochemical and structural evidence, both T7 gp4 and mtDNA helicase form hexamers or heptamers in solution (7, 14–17). Moreover, the secondary and tertiary structure of mtDNA helicase is also similar to that of T7 gp4; both contain distinct N and C termini separated by a flexible linker (9). The C-terminal domain in both proteins harbors the active site responsible for NTPase activity, and can unwind duplex DNA substrates independent of the N-terminal domain (18). Both helicases are members of the DnaB-like family of replicative DNA helicases, which can form ring-shaped hexamers that encircle the DNA substrate (19). The linker region is important for the hexamerization of the T7 gp4 (20). The N-terminal regions of the metazoan replicative mtDNA helicases share primary and secondary sequence conservation with the primase domain of bacteriophage T7 gp4 and with bacterial

\* This work was supported, in whole or in part, by National Institutes of Health Grant GM45295 (to L. S. K.).

<sup>1</sup> Recipient of a career development award from the office of the Vice President for academic affairs at Birzeit University.

<sup>2</sup> To whom correspondence should be addressed. Tel.: 517-353-6703; Fax: 517-353-9334; E-mail: Iskaguni@msu.edu.

DnaG primases (21), and all carry two subdomains, a zinc-binding domain (ZBD)<sup>3</sup> and an RNA polymerase domain (RPD) (22, 23). Although the prokaryotic forms catalyze DNA primase activity, metazoan mtDNA helicase lacks a primase function as a result of the loss of key active site residues in the RPD (21). In contrast to those of other metazoans, insect mtDNA helicases retain conserved cysteine residues in the ZBD region, which serve to coordinate zinc in T7 gp4. We report here that the isolated N-terminal domain of *Drosophila melanogaster* mtDNA helicase (NTD) binds an iron-sulfur cluster that increases the stability of the isolated protein *in vitro*. We demonstrate that the Fe-S liganding residues correspond to the residues in T7 gp4 that coordinate zinc. Moreover, we show that the *Drosophila* NTD binds DNA.

## EXPERIMENTAL PROCEDURES

**Materials**—Nickel-nitrilotriacetic acid (Ni-NTA)-agarose resin was purchased from Qiagen (Valencia, CA); most other reagents were purchased from Sigma, including bovine serum albumin (BSA), cytochrome *c*,  $\beta$ -mercaptoethanol,  $\text{Fe}(\text{NO}_3)_3 \cdot 9\text{H}_2\text{O}$ ,  $\text{Na}_2\text{S}$ , and  $\text{NaBH}_4$ . Fluorescein-labeled and unlabeled DNA oligomers were obtained from IDT (Coralville, IA); glycerol and  $\text{H}_2\text{O}_2$  were from J.T. Baker (Phillipsburg, NJ). Precision protein markers were from Bio-Rad. Dithiothreitol was purchased from Research Organics (Cleveland, OH).

**Cloning and Mutagenesis of the Dm Mitochondrial DNA Helicase NTD (Asn<sup>24</sup>-Ala<sup>333</sup>)**—Helicase variants were constructed via site-directed PCR mutagenesis of the NTD open reading frame cloned into the plasmid pET28a, with an N-terminal hexahistidine tag. The engineered NTD sequence is as follows: **MGHHHHHAT**<sup>24</sup>NYATQVVSGLEECSLDPKEYVDFKRLRQLNLPKDGHTCLQLECRLCDNRNRPVTNAQKGTDHGLLAYVNRKTGAFICPNCVKTSLTSALLSYQLPKP<sup>123</sup>VGKQPLQRQPVYESRPHLAVVTPEACAA-LGIKGLKEDQLNAIGAQWEPQQQLLHFKLNRNAAQVEV-GEKVLVYLGDRREEIFQSSSSGLLIHGAMNKTKAVLVS-NLIDFIVLATQNIETHCVVCLPYELKTLPQECLPALERF-KELIFWLHYDASHSWDAARAFALKLDERRCLLIRPTET-EPAPHLALRRRLNLRHILAKATPVQHKA<sup>333</sup>. The first 10 residues shown in bold represent the added N-terminal tag. The underlined segment indicates the ZBD portion of the NTD. The superscript numbers correspond to the amino acid residue numbers in the native protein. The molecular mass of the engineered protein was calculated to be 36283.8 Da with a pI of 8.81 using the ProtParam tool (24). The molar extinction coefficient for the NTD at 280 nm was calculated to be  $29,910 \text{ M}^{-1} \text{ cm}^{-1}$ . This value was used in the determination of concentration from  $A_{280}$  data. PCRs were performed using the Expand Long PCR System (Roche Applied Science) and standard laboratory methods. The oligonucleotides used for PCR were: 5'-CAAAGACGGACACACGgcCTTGACGCTGGAGTGT-3' and 5'-ACACTCCAGCTGCAAGgcCGTGTGTCGGTCTTTG-3' for

NTD C63A; 5'-GCTTGCAGCTGGAGgcTCGCCTCgcCGA-TCGCAATAGGC-3' and 5'-GCCTATTGCGATCgGAG-GCGAgcCTCCAGCTGCAAGC-3' for NTD C68A/C71A; 5'-CGGACGGGAGCCTTTATCgcCCCCAATgcCGACGTAA-AAACCTC-3' and 5'-GAGGTTTTTACGTCGgcATTGGG-GgcGATAAAGGCTCCCGTCCG-3' for NTD C102A/C105A; 5'-GCCACACAGAACATTTGAAACGCATgcCGTTGTAgc-CCTGCCCTACGAACT-3' and 5'-AGTTCGTAGGGCAGG-gcTACAACGgcATGCGTTTTCAATGTTCTGTGTGGC-3' for NTD C245A/C248A; 5'-GACTCTACCACAAGAGgcTC-TGCCCGCCTTCGAA-3' and 5'-TTCCAAGGCGGGCAGA-gcCTCTTGTGGTAGAGTC-3' for NTD C260A; and 5'-TAAAGTTGGACGAAAGGCGAgcCCTGTTAATCCGAC-CTAC-3' and 5'-GTAGGTCGGATTAACAGGgcTCGCCT-TTCGTCCAACCTTA-3' for NTD C297A. The lowercase letters indicate the sites where mutations were introduced to create alanine substitutions.

**Protein Overexpression and Purification of Dm mtDNA Helicase NTD**—*Escherichia coli* expressing *Dm* mtDNA helicase and its variants were grown in Luria broth (1 liter) at 37 °C and induced with isopropyl thiogalactoside at 16 °C overnight by standard methods. Cells were harvested by centrifugation and washed with an equal volume of cold Tris sucrose buffer (50 mM Tris-HCl, pH 7.5, 1 mM phenylmethylsulfonyl fluoride (PMSF), 10 mM sodium metabisulfite, 2  $\mu\text{g}/\text{ml}$  of leupeptin, 10% sucrose, and 5 mM  $\beta$ -mercaptoethanol), recentrifuged, frozen in liquid nitrogen, and stored at  $-80^\circ\text{C}$ . The frozen cell pellets were thawed on ice, and all further steps were performed at 0–4 °C. Cells were suspended in 1/25 volume of the original cell culture in Tris sucrose buffer. Cells were lysed by addition of 5 $\times$  lysis buffer (1.25 M NaCl, 7.5% *n*-dodecyl  $\beta$ -D-maltoside, 5 mM 2-mercaptoethanol) to 1 $\times$  final concentration, followed by a freeze-thaw cycle. The resulting lysate was centrifuged and the soluble extract (fraction I, 300–350 mg of proteins) was loaded onto a Ni-NTA-agarose column (5.0 ml of resin/liter of cells) equilibrated with buffer containing 50 mM Tris-HCl, pH 7.5, 0.5 M KCl, 10% glycerol, 15 mM imidazole, 1 mM PMSF, 10 mM sodium metabisulfite, 2  $\mu\text{g}/\text{ml}$  of leupeptin, and 5 mM 2-mercaptoethanol. The column was washed sequentially with buffers containing 15, 20, and 100 mM imidazole, and the bound protein was eluted with buffers containing 200 and 500 mM imidazole. Fractions were analyzed by SDS-PAGE and recombinant proteins were pooled accordingly as fraction II (4–6 mg of protein). Fraction II was loaded on linear 12–30% glycerol gradients prepared in 35 mM Tris-HCl, pH 7.5, 250 mM NaCl, 5 mM  $\beta$ -mercaptoethanol, and gradients were centrifuged at  $180,000 \times g$  for 70 h at 4 °C in a Beckman SW40 rotor. Gradients were fractionated, analyzed by 12% SDS-PAGE, and fractions were pooled according to purity (fraction III, 3.5–8 mg of protein), frozen in aliquots in liquid nitrogen, and stored at  $-80^\circ\text{C}$ .

**Trypsin Proteolysis**—The purified NTD (3  $\mu\text{g}$ ) was subjected to proteolysis with trypsin (0.6  $\mu\text{g}$ , Sigma) for 10 min at 20 °C in a buffer containing 50 mM Tris-HCl, pH 8.0, 4 mM  $\text{MgCl}_2$ , 10% glycerol, 2 mM  $\beta$ -mercaptoethanol. The reaction was terminated with soybean trypsin inhibitor (1.2  $\mu\text{g}$ , Sigma), and the products were analyzed by 17% SDS-PAGE.

<sup>3</sup> The abbreviations used are: ZBD, zinc binding domain; T7 gp4, bacteriophage T7 gene 4 protein primase-helicase; RPD, RNA polymerase domain; NTD, N-terminal domain; Ni-NTA, nickel-nitrilotriacetic acid; GFAA, graphite furnace atomic absorption; ssDNA-FI, fluorescein-labeled single-stranded DNA oligomer.

## Dm mtDNA Helicase Contains an Fe-S Cluster

**Ultraviolet-Visible Spectroscopy**—Electronic spectra were obtained on a Hewlett-Packard 8453 spectrophotometer, in a quartz cuvette with a 1-cm path length. The spectrophotometer was zeroed with 35 mM Tris-HCl, pH 7.5, 250 mM NaCl, 12% glycerol, 5 mM  $\beta$ -mercaptoethanol.

**Determination of Biological Iron by Graphite Furnace Atomic Absorption (GFAA) Spectroscopy**—A Hitachi Z-9000 GFAA spectrometer was used for iron determination. Protein samples (3.9 to 7.8 nmol) were oxidized and digested in 0.5 ml of 70% HNO<sub>3</sub> and 0.5 ml of 30% H<sub>2</sub>O<sub>2</sub>. The samples were boiled in a water bath with boiling chips until more than 90% of the original sample volume was evaporated. 2% HNO<sub>3</sub> (2 ml) was added and the tubes were capped with parafilm until analyzed. Iron standard solutions were prepared from a 1 mM iron(III) nitrate nonahydrate solution containing 2% HNO<sub>3</sub>, 12 mM Tris-HCl, 0.2 mM EDTA, 3.5% glycerol. The blank solution contained only the components of the buffer. Standard solutions and digested samples were analyzed in triplicate in the GFAA spectrometer using a drying temperature of 80–120 °C for 30 s, ashing temperature of 630 °C for 30 s, and an atomization temperature of 2700 °C for 10 s. Absorbance values were recorded at a wavelength of 248.3 nm.

**Determination of Protein Sulfide Content by Methylene Blue Photometric Assay**—Protein samples (0.8 to 2 nmol) were diluted in microcentrifuge tubes to 100  $\mu$ l with water. 1% Zinc(II) acetate dihydrate (300  $\mu$ l) was added to each sample followed by the immediate addition of 15  $\mu$ l of 12% NaOH. The tubes were kept at room temperature for 30 min, with occasional mixing of the tubes by inversion. The ensuing suspension was subsequently underlaid with 75  $\mu$ l of 0.1% *N,N*-dimethyl-*p*-phenylenediamine in 5 M HCl. 23 mM FeCl<sub>3</sub> in 1.2 M HCl (30  $\mu$ l) was added to the bottom layer, and the solution was mixed by inversion. The tubes were then centrifuged at 2000  $\times$  *g* for 20 min. The absorbance of the supernatant at 670 nm was measured, and the amount of sulfide was calculated from a standard curve that was generated by dilution of 1 mM Na<sub>2</sub>S $\cdot$ 9H<sub>2</sub>O in 0.1 M NaOH to give concentrations ranging from 0.5 to 5 nmol of S<sup>2-</sup>.

**Determination of Protein Secondary Structure by Circular Dichroism (CD)**—Circular dichroic spectra for all proteins were determined in a quartz cuvette (0.1 cm path length) using a Chirascan CD spectropolarimeter equipped with a temperature-controlled cell holder from Applied Photophysics. NTD proteins were dialyzed in buffer containing 35 mM Tris-HCl, pH 7.5, 250 mM NaCl, 12% glycerol, 10 mM  $\beta$ -mercaptoethanol in Slide-A-Lyzer G2 MWCO 10,000 dialysis cassettes; ZBD was dialyzed in Spectra/Por MWCO 6,000–8,000 dialysis membrane. The starting protein concentration was  $\sim$ 0.75 mg/ml. The samples were dialyzed for 2 h in 500 ml of buffer at 4 °C. The buffer was exchanged and the samples were dialyzed further overnight at 4 °C. The concentrations of the resulting dialyzed proteins were measured and adjusted (by dilution, or by concentration using Amicon Ultra 10 K centrifugal filters) to final concentrations of  $\sim$ 0.3 mg/ml. UV-visible spectra were taken, and the CD spectra for all samples were obtained immediately thereafter. Three spectra per protein were obtained. This process was repeated with a second preparation of each

protein, and the spectra from both sets of purifications were averaged and presented here.

**Determination of the Nature of the Iron-Sulfur Cluster by Electrospray Ionization Mass Spectrometry**—Protein samples were dialyzed in 10 mM NH<sub>4</sub>HCO<sub>3</sub>, pH 8.5, 12% glycerol, 10 mM  $\beta$ -mercaptoethanol for 2 h at 4 °C, and again overnight after buffer was exchanged. UV-visible spectra of the resulting dialyzed proteins were obtained, and the protein samples were then subjected to analysis using online desalting in a Waters Xevo G2-S Q-TOF Mass Spectrometer in positive ion mode. The multiply charged electrospray ionization mass spectra were deconvoluted to zero charge state spectra using the MaxEnt1 feature of Waters MassLynx version 4.1 software.

**Determination of NTD Protein Stability by Differential Scanning Calorimetry**—Protein samples were prepared as for CD analysis, frozen in liquid nitrogen, and stored at  $-80$  °C prior to analysis in a capillary VP-DSC instrument (GE Healthcare). Proteins were diluted directly into a 96-well plate to a final concentration of 0.15 mg/ml with the same buffer in which they were dialyzed (35 mM Tris, pH 7.5, 200 mM NaCl, 12% glycerol and 10 mM  $\beta$ -mercaptoethanol). The proteins were scanned at a scan rate of 120 °C/h, over a temperature range from 20 to 120 °C.

**Fluorescence Quenching as a Measure of DNA Binding by NTD and Its Variants**—The fluorescence intensity of a fluorescein-conjugated single-stranded DNA 40-mer (ssDNA-FI, 5'-ATTA[Fl~T]GAATTAATTTAATAATTTTTTTTTTTTTTTT-TTTTTT-3') was measured from 500 to 550 nm in a Jobin Yvon Spex Fluorolog-3 spectrofluorometer equipped with a thermostated cell holder. The excitation wavelength for the fluorophore was 480 nm and the measuring temperature was 22 °C. The working solution was 10 nM ssDNA-FI in 50 mM Tris-HCl, pH 7.5. 10 nM ssDNA-FI (500  $\mu$ l) was added to a quartz cuvette (0.5-cm path length) and the fluorescence spectrum was recorded. Successive additions of proteins (1–5  $\mu$ l) were made, and the spectra were recorded after an incubation time of 2 min to equilibrate the protein and DNA. The addition of similar volumes of buffer alone was used as a control. For the fluorescein only control, 3.5 nM fluorescein (500  $\mu$ l in 50 mM Tris-HCl pH 7.5) was used instead of ssDNA-FI, followed by similar additions of NTD. In the analysis of salt sensitivity, various amounts of 3 M NaCl were added after achieving quenching of fluorescence with 500 nM NTD, followed by measurement of the fluorescence spectra.

## RESULTS

**N-terminal mtDNA Helicase Constructs Designed via Bacteriophage T7 gp4 Homology**—To study the function of the N-terminal domain of metazoan mtDNA helicase, two constructs of *D. melanogaster* mtDNA helicase were produced (Fig. 1). The first construct, termed NTD, comprises residues Asn<sup>24</sup>-Ala<sup>333</sup>. This region in bacteriophage T7 gp4 contains the conserved ZBD and RNA polymerase domain (RPD). The second construct comprising residues Asn<sup>24</sup>-Pro<sup>123</sup> contains only the conserved ZBD. N-terminal His<sub>6</sub> tags were added to both constructs and their expression was induced in *E. coli* (see “Experimental Procedures”).

**Purification and Physical Characterization of the NTD *Dm* mtDNA Helicase**—Our laboratory has previously isolated and characterized the full-length human mtDNA helicase (14), and a similar purification strategy was adopted for the *D. melano-*

*gaster* constructs. To that end, a soluble extract of His-tagged NTD (fraction I) was purified to near-homogeneity by Ni-NTA column chromatography (fraction II), followed by velocity sedimentation in glycerol gradients (fraction III). The purified protein (3.5–8 mg of protein/liter of cell lysate) sedimented with a coefficient of 2.9 S (Fig. 2A), indicating that the isolated NTD is a monomer. SDS-PAGE of fraction III resulted in a single band of molecular mass of ~36,000 Da (Fig. 2B), consistent with the calculated mass of 36283.8 Da (see “Experimental Procedures”).

**NTD Has a T7 Primase Helicase-like Modular Architecture**—The physical architecture of purified NTD was probed by proteolysis with trypsin, yielding two stable fragments of 10 and 26 kDa (Fig. 3A). An immunoblot using anti-His antibody identified the 10-kDa band as the N-terminal fragment, whereas the

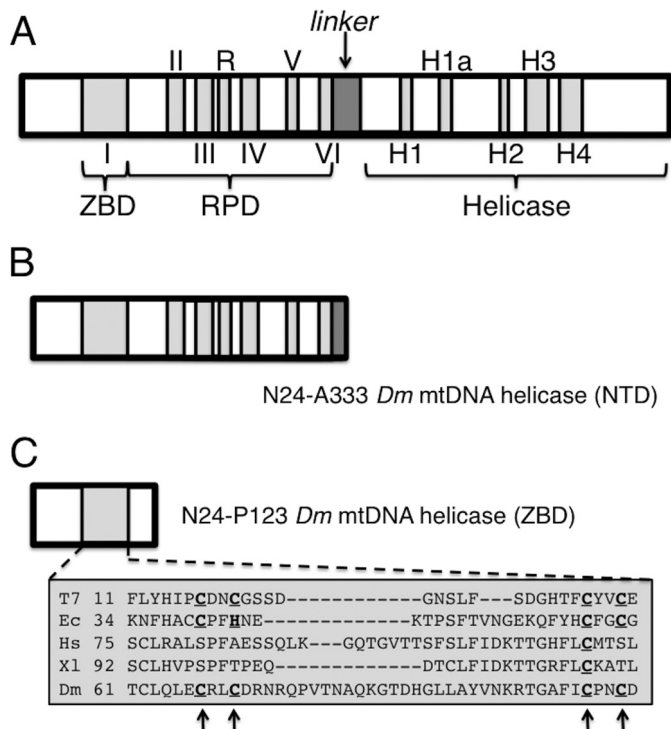


**FIGURE 1. Motifs of the *Dm* mtDNA helicase based on bacteriophage T7 gp4 amino acid sequence homology.** A, a schematic representation of the amino acid sequence motifs of *Dm* mtDNA helicase showing a linker region separating the C-terminal domain (helicase domain) from the N-terminal domain (zinc binding and RNA polymerase domains). Schematic diagrams of the N-terminal protein constructs studied in this report are shown: the NTD, 36 kDa, amino acids Asn<sup>24</sup>-Ala<sup>333</sup> (B) and ZBD, 12 kDa, amino acids Asn<sup>24</sup>-Pro<sup>123</sup> (C). Multiple sequence alignment of the zinc-binding motif I, with arrows indicating the positions of four conserved cysteine residues that ligate zinc in T7 gp4.

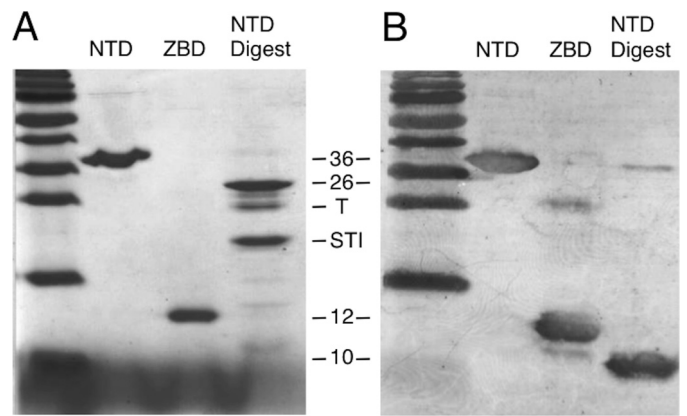


**FIGURE 3. Trypsin digestion of NTD confirms an architecture similar to T7 gp4 primase-helicase.** Purified NTD (fraction III) was digested with trypsin (see “Experimental Procedures”), and the digest was analyzed by 17% SDS-PAGE. Undigested, purified NTD and ZBD were electrophoresed as controls. The gel was stained with Coomassie Blue (A) or transferred to a nitrocellulose membrane and immunoblotted with anti-His antibody (B). Precision Plus Protein Standards (Bio-Rad) were electrophoresed in the first lane, and the sizes of species identified in the experimental lanes are indicated between panels A and B. T indicates the migration position of trypsin, and STI that of soybean trypsin inhibitor.

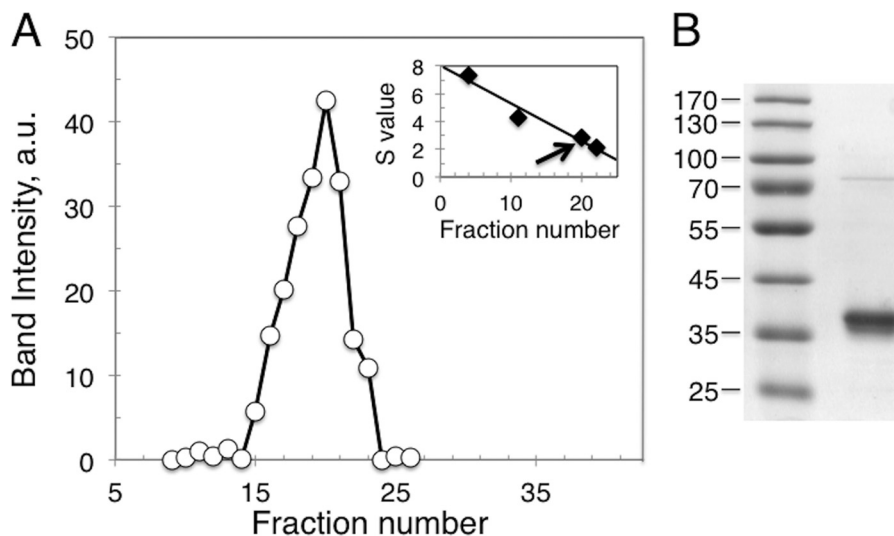


**FIGURE 2. Hydrodynamic analysis of NTD.** A, Ni-NTA-purified NTD was sedimented in a 12–30% glycerol gradient, and fractions were analyzed by 10% SDS-PAGE and Coomassie Blue staining. The inset represents a calibration graph of standard protein markers, which were run in a parallel gradient (rabbit muscle L-lactate dehydrogenase, 7.35 S; human serum albumin, 4.3 S; carbonic anhydrase, 2.8 S; cytochrome c, 2.1 S). The arrow points to the sedimentation position of NTD at 2.9 S. B, Coomassie Blue stained, 10% SDS-polyacrylamide gel showing a typical glycerol-gradient purified NTD (fraction III), migrating with a molecular mass of 36 kDa, right lane. The sizes of Precision Plus Protein standards (Bio-Rad), electrophoresed in the left lane are indicated.

## Dm mtDNA Helicase Contains an Fe-S Cluster

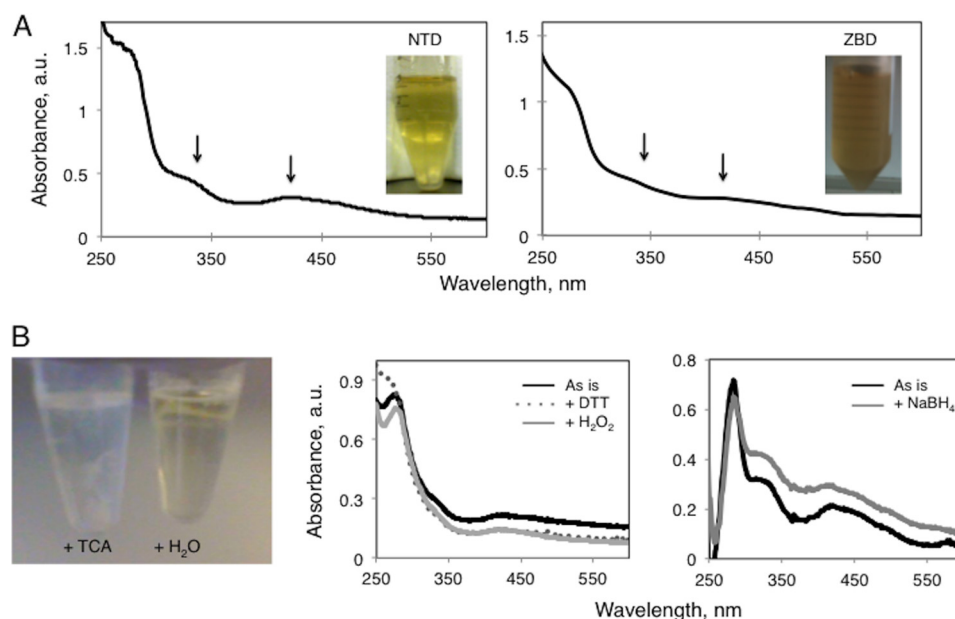


FIGURE 4. **Spectral characteristics of NTD and ZBD.** *A*, both isolated proteins are colored: glycerol-gradient purified NTD (fraction III) is golden brown (*left*) and a cell lysate of bacteria overexpressing the ZBD (fraction I) is intensely brown (*right*). The UV-visible spectra of NTD (fraction III, *left*) and ZBD (fraction III, *right*) show a shoulder at 325 nm and a small peak at 422 nm (indicated by *arrows*) that are characteristic of proteins binding iron-sulfur clusters. *B*, *left*, treatment of purified NTD (5  $\mu$ M, 100  $\mu$ l) with 10% TCA (100  $\mu$ l) immediately produces a colorless solution with precipitating white crystals, whereas addition of 100  $\mu$ l of water only dilutes the color. *Middle*, addition of reducing agent (10 mM DTT) or oxidizing agent (10 mM H<sub>2</sub>O<sub>2</sub>) to purified NTD (30  $\mu$ M) had no apparent effect on the spectral properties of the protein. *Right*, addition of 1 mM NaBH<sub>4</sub> to purified NTD (25  $\mu$ M) does not bleach the peak at 422 nm, indicating that the cofactor is an Fe-S cluster rather than pyridoxal 5'-phosphate.

26 kDa fragment was not detected (Fig. 3B). These results confirm that the NTD construct adopts a similar domain architecture as that of T7 gp4, which contains an N-terminal ZBD tethered flexibly to a larger RPD. Trypsin digestion was also performed in the presence of DNA and RNA substrates, but no change in the digestion profile was observed (data not shown). We observed that the ZBD proteolytic fragment of the NTD is somewhat smaller than the engineered construct, indicating that the engineered construct carries part of the linker between the ZBD and RPD.

**Spectral Characteristics of the NTD and ZBD Dm mtDNA Helicases**—Lysis of bacterial cells overexpressing the NTD gives rise to a golden brown solution, and this color is retained upon further purification (Fig. 4A, *inset at left*). Upon treatment with 10% trichloroacetic acid, the color disappears immediately and the precipitating crystals are *white* (Fig. 4B, *left*), suggesting that the purified protein contains an acid-labile form of bound iron. To verify this, UV-visible electronic absorption spectra of the purified protein were obtained. The spectra show regions characteristic of iron-sulfur-binding proteins, with a significant shoulder at  $\sim$ 325 nm and a broad peak at  $\sim$ 422 nm (Fig. 4A, *left*). Incubation of the purified NTD with various redox molecules does not change substantially the spectral pattern, and hence does not disrupt the putative iron-sulfur cluster (Fig. 4B, *middle*). Enzymes containing another cofactor, pyridoxal 5'-phosphate, are golden brown and show an absorbance peak at 425 nm. However, pyridoxal 5'-phosphate enzymes are bleached with NaBH<sub>4</sub> and the 425 nm peak is lost (25, 26). Addition of NaBH<sub>4</sub> to the purified NTD did not bleach the 422-nm peak, confirming that the color is due to the presence of an iron-sulfur cluster (Fig. 4B, *right*).

Similar to the NTD, lysates of bacterial cells expressing the ZBD construct appear dark brown (Fig. 4A, *inset at right*) and upon further purification, the ZBD protein retains the color, albeit at a lower intensity. UV-visible spectra of the purified ZBD protein show the expected iron-sulfur shoulder at 325 nm and broad peak at 422 nm (Fig. 4A, *right*).

**Both NTD and ZBD Contain Iron and Sulfide**—To investigate further the presence of an iron-sulfur cluster, the iron and sulfide contents of numerous purifications of the NTD and ZBD were determined. Iron content was quantified by GFAA spectrometry after nitric acid digestion of the purified proteins (see "Experimental Procedures"). Purified NTD contains  $1.6 \pm 0.3$  iron atoms per protein molecule (mean  $\pm$  S.D. of four different preparations). We also found colorimetric iron detection assays to produce similar values, albeit less reproducibly as compared with the GFAA analysis (data not shown). Sulfide content was determined by colorimetric assay using the methylene blue method (27). Purified NTD proteins contain  $2.2 \pm 0.2$  sulfide ions per protein molecule (mean  $\pm$  S.D. of four different preparations). Together, these data demonstrate that the NTD contains an iron-sulfur cluster, and suggest it is a 2Fe-2S cluster. However, the data do not discriminate definitively between the possible 2Fe-2S, 2Fe-3S, or 4Fe-4S types.

The iron and sulfide content in the ZBD was examined, and the ZBD was also found to contain both elements, although the highest ratio of iron and sulfide atoms to protein obtained was  $\sim$ 0.9. Furthermore, and in contrast to the robust NTD, purified ZBD is unstable at 4  $^{\circ}$ C, as evidenced by the appearance of substantial aggregation after only 3 h post-purification. Interestingly, both the purified NTD and ZBD were shown to be devoid of zinc: we found that their zinc content was not statistically

different from the background by atomic absorption spectroscopy (data not shown). The lack of zinc argues that the ZBD in *Drosophila* mtDNA helicase does not bind zinc as does its counterpart in T7 gp4; rather our findings suggest that the iron-sulfur binding site lies within the ZBD.

**Identification of Iron-Sulfur Ligands in the Dm NTD**—An iron-sulfur center is typically ligated by four cysteine residues. In insect mtDNA helicases, each of the four cysteines that have been shown to bind zinc in T7 gp4 are conserved. In contrast, only one of these is conserved in vertebrate metazoans (Fig. 1C). Interestingly, we have not observed a brown color in the human mtDNA helicase, and it does not have the characteristic UV-visible spectrum of iron-sulfur proteins (data not shown). Based on amino acid sequence alignments we targeted these four conserved cysteines, as well as several more C-terminal conserved cysteines for alanine substitution mutagenesis. Six variants were constructed and produced in *E. coli* (Fig. 5). Three contain single alanine substitutions (C63A, C260A, and C297A), and three are double substitutions (C68A/C71A, C102A/C105A, and C245A/C248A). The single alanine variants were selected



**FIGURE 5. Mutagenesis of the NTD to identify the Fe-S binding residues.** The sequence of NTD is presented with the positions of cysteines mutated to alanine in numbered boxes. The underlined portion of the sequence represents the engineered ZBD moiety of the NTD. Three NTD double substitution variants (C68A/C71A, C102A/C105A, and C245A/C248A) and three single substitutions (C63A, C260A, and C297A) were engineered. Three substitutions map to within the ZBD, and three are within the RPD.

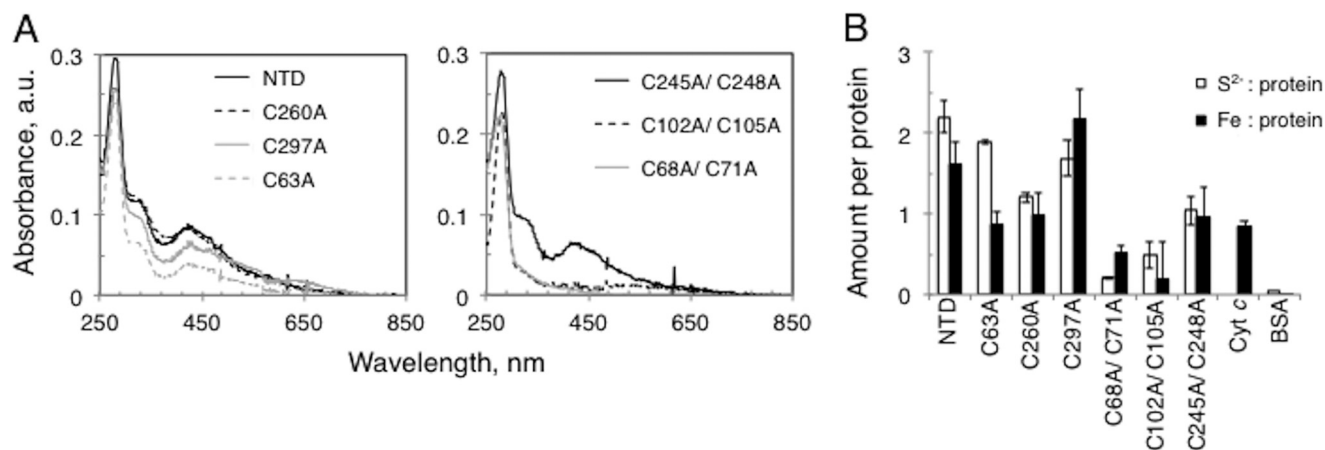


**FIGURE 6. Spectral and biochemical properties of NTD variants.** All NTD variants were expressed and purified to near-homogeneity, and their spectral properties assessed. *A*, proteins (10  $\mu$ M) were subjected to UV-visible analysis. The left panel shows NTD and single substitution variants, and the right panel shows proteins with double substitutions. *B*, elemental analysis of the NTD proteins by colorimetric detection (for sulfide content) and graphite furnace atomic absorption (for iron content) confirm the presence of at least one iron atom and one sulfide ion per protein, except for the double mutants in the ZBD. The data represent the average and S.D. of three biological replicates.

## Dm mtDNA Helicase Contains an Fe-S Cluster

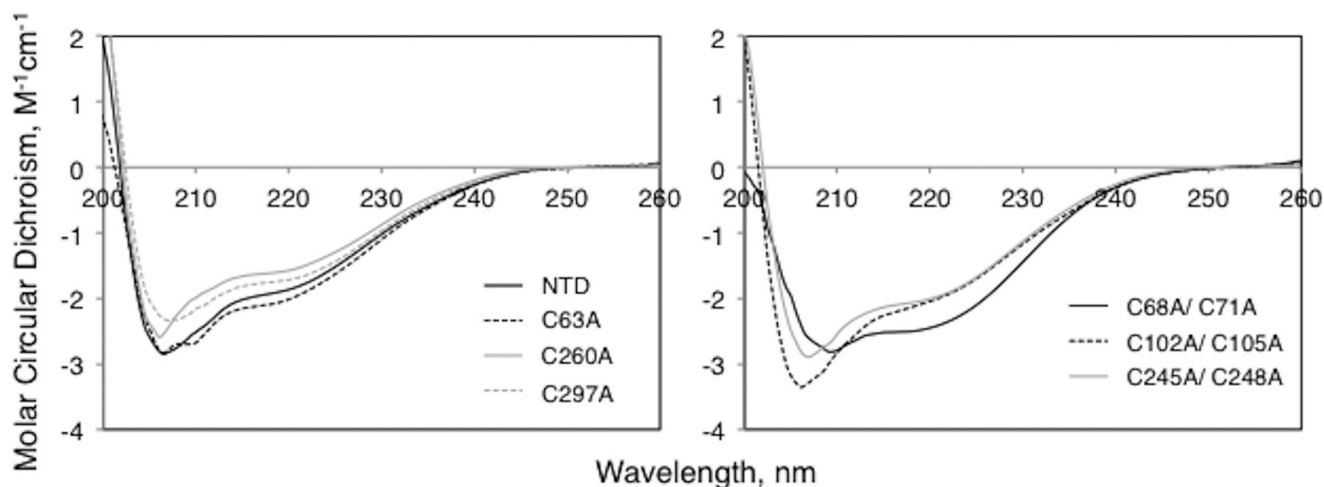


FIGURE 7. **Circular dichroism of NTD proteins.** NTD protein and its variants were subjected to buffer exchange by dialysis (see “Experimental Procedures”). The protein concentrations were then determined and the NTD proteins were adjusted to 0.32 mg/ml prior to determination of CD spectra. NTD and single substitution variants are shown at *left*, and the doubly substituted NTD proteins are shown at *right*. The graphs are the average traces of two biological replicates, each consisting of three replicate measurements.

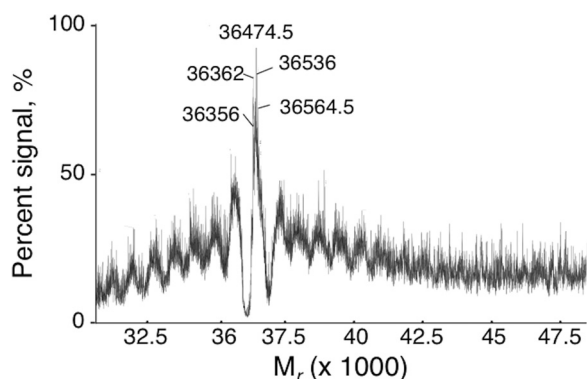


FIGURE 8. **Mass spectrometry confirms the presence of an iron-sulfur center in NTD.** Purified NTD was subjected to buffer change by dialysis (see “Experimental Procedures”), analyzed by positive mode electrospray ionization, and the spectrum was converted to the zero charge state spectrum shown using MaxEnt1 algorithms. A representative trace of NTD mass shows five distinct masses in the main peak.

trometry to determine the mass of the intact protein from five independent preparations. The theoretical mass of the NTD including amino acid residues Asn<sup>24</sup>-Ala<sup>333</sup> plus the His tag is 36,283.8 Da (see “Experimental Procedures”). Fig. 8 shows a representative mass peak profile of the NTD. In all five preparations, the mass values observed were consistently higher than the theoretical mass of the NTD. There were multiple incidences of a mass difference of  $82.7 \pm 4.3$  (consistent with the presence of 1 Fe and 1 S per protein,  $M_r = 87.9$ ) and  $184.8 \pm 5.9$  (consistent with a 2Fe-2S,  $M_r = 175.8$ ). Higher mass differences were not observed consistently, indicating that the NTD is unlikely to bind a cluster larger than 2Fe-2S.

Mass spectrometric analysis was also performed on two purifications of the ZBD and the non-iron-sulfur containing double alanine variants. Consistent with the iron and sulfide determinations, the ZBD gave rise to peaks indicative of the presence of 1 Fe and 1 S per protein ( $93.1 \pm 6.9$  Da). In contrast, the peaks observed for the NTD double alanine variants were consistent with the theoretical mass of the apoprotein, and there were no peaks observed with higher masses in any of the scans, confirming the absence of an iron-sulfur cluster in these variants.

Taken together, these data document the presence of a 2Fe-2S cluster in the NTD. The colorless variants lack evidence of the cluster, corroborating the identification of the coordinating cysteine ligands.

*A Role for the Iron-Sulfur in Protein Stability*—We next investigated the role of the iron-sulfur cluster in the NTD by subjecting the purified protein samples to differential scanning calorimetry. We found that the  $T_m$  values for all of the proteins except the non-iron-sulfur containing variants are  $>50^\circ\text{C}$ , whereas the C102A/C105A showed a consistently lower  $T_m$  ( $\sim 47^\circ\text{C}$ ) suggesting that it is less stable than the others, and the C68A/C71A variant proved to be unstable under the conditions of the analysis to determine reliably the  $T_m$ . This was also apparent by measuring the absorbance of the NTD proteins at 280 nm as a function of time. The absorbance of the NTD declines only slightly over 20 h on ice; conversely, the absorbance of both double variants that do not contain the Fe-S cluster drops precipitously to 40–50% within 2 h, declining to 20–25% over 20 h (data not shown).

*The NTD of Dm mtDNA Helicase Binds DNA*—Investigating the functional role of the NTD in metazoan mtDNA helicases is difficult because there is no known activity to assess. However, based on the function of the RPD in T7 gp4, we explored a possible role for the NTD in DNA binding. To do so, we used a fluorescence quenching assay with a fluorescein-labeled single-stranded DNA oligomer (ssDNA-Fl, see “Experimental Procedures”). We found that addition of NTD to a ssDNA-Fl-containing solution results in a dose-dependent quenching of its initial fluorescence (Fig. 9, *top left*). Quenching is reversible by the addition of NaCl in a dose-dependent manner (Fig. 9, *bottom right*), as restoration of the initial fluorescence is achieved using either NaCl or  $\text{MgCl}_2$  (data not shown), indicating that the binding is electrostatic in nature. At the same time, addition of NTD to fluorescein alone does not cause a change in the fluorescence, indicating that the effect is DNA specific (Fig. 9, *bottom left*). Likewise the addition of cytochrome *c* to ssDNA-Fl does not cause any change in the fluorescence pattern, arguing that the effect is protein specific (Fig. 9, *bottom center*). All

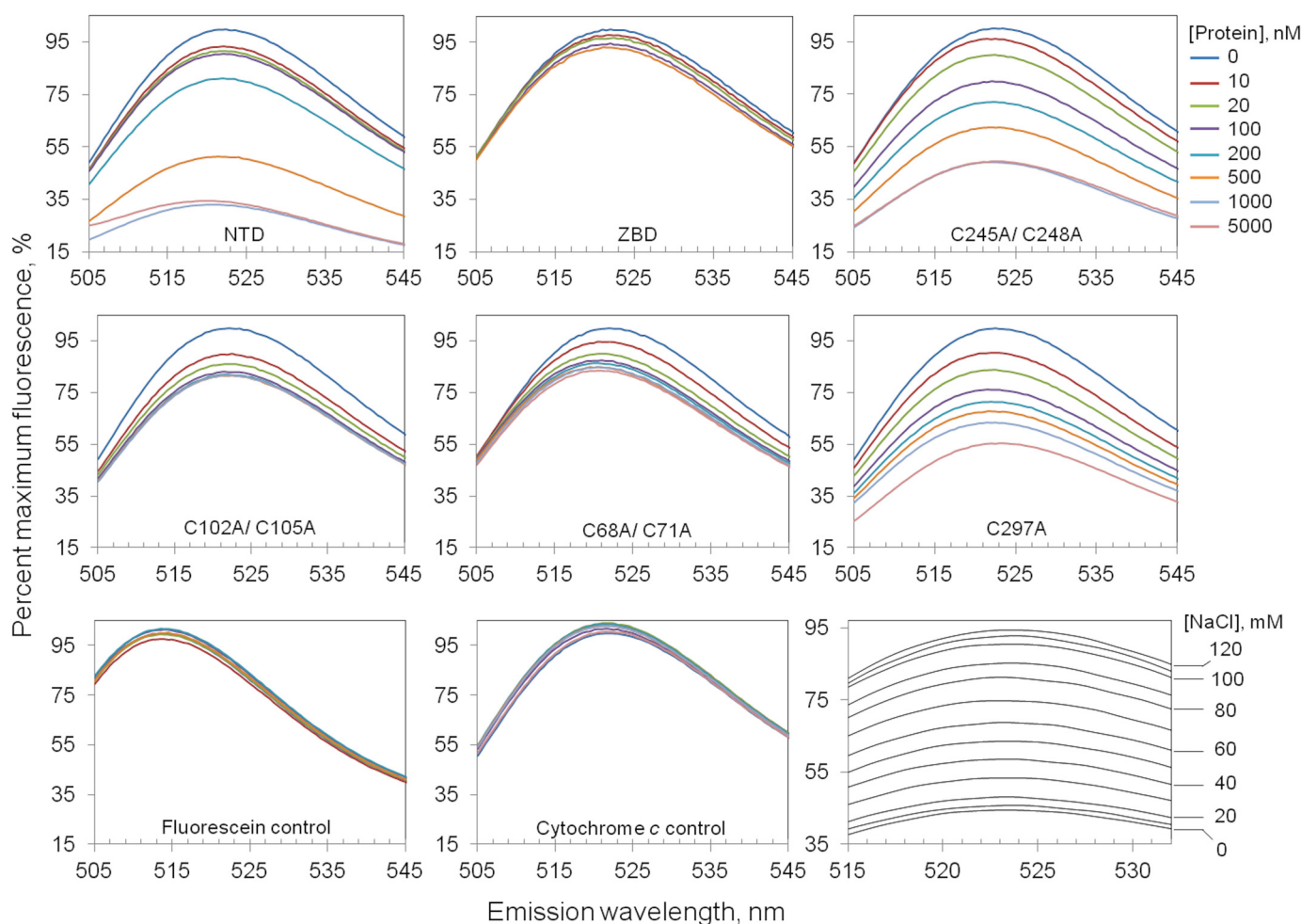


**FIGURE 9. NTD binds a fluorescein-labeled, single-stranded oligonucleotide.** NTD proteins were assessed for their ability to bind ssDNA (see “Experimental Procedures” for the oligonucleotide sequence). The fluorescence of a 10 nM solution of ssDNA-FI was measured with sequential protein additions. *Upper and middle rows*, the addition of NTD proteins led to the quenching of fluorescence suggesting DNA binding, whereas quenching was not observed for the ZBD. *Bottom row, left and center panels*, control experiments were performed with NTD and 10 nM free fluorescein (no DNA), and with ssDNA-FI and cytochrome *c*, respectively. *Bottom right panel*, sequential addition of NaCl to the NTD-ssDNA-FI samples eliminates fluorescence quenching. 500 nM NTD was allowed to quench 10 nM ssDNA-FI in the absence of NaCl prior to the addition of NaCl. The final concentrations are shown in 10 mM increments.

purified NTD variants showed DNA binding with varying affinities ( $K_d$  ranging from 120 to 200 nM for all variants), except for the ZBD alone. However, the absence of the iron-sulfur cluster in the double alanine variants in the ZBD does not permit a direct comparison of their DNA-binding affinities to the Fe-S-containing forms, because they must be exhibiting fluorescence quenching by a mechanism other than the Förster resonance transfer mechanism, which predominates in the latter (31). Nonetheless, the C68A/C71A and C102A/C105A variants do exhibit quenching (Fig. 9, *middle left and center panels*), indicating that the Fe-S cluster is not essential for DNA binding. (We evaluated their DNA binding properties by fluorescence anisotropy but failed to obtain reliable data, presumably due to their relative instability as compared with other constructs, data not shown.) Fluorescence quenching was lost (and fluorescence signals restored) when an unlabeled oligomer was added to the preformed NTD·DNA-FI complexes (data not shown). We also found that the NTD bound both single-stranded and double-stranded DNA oligomers with similar affinity (data not shown).

In composite, our results suggest a functional role for the NTD in DNA binding. The calculated affinity of the NTD for DNA obtained by this method ( $K_d \sim 120$  nM) is considerably lower than that of the full-length human mtDNA helicase, which binds DNA tightly in its C-terminal helicase domain ( $K_d = 6$  nM ((32)).

## DISCUSSION

Mitochondrial DNA helicase is a fundamental part of the minimal mitochondrial replisome (5) and its activity is required for the maintenance of mtDNA *in vivo* (7, 9–13). The C-terminal domain of the helicase catalyzes its NTPase and DNA unwinding activities as in bacteriophage T7 gp4 primase-helicase (18, 33). In contrast, whereas the N-terminal domain of bacteriophage T7 gp4 catalyzes DNA primase activity, metazoan mtDNA helicase has lost critical residues required for this activity, despite sharing substantial sequence homology with T7 gp4 (21). Nonetheless, the NTD is strongly conserved throughout metazoa (10) and a number of pathogenic alleles have been identified in the human NTD (34, 35). Furthermore,

## Dm mtDNA Helicase Contains an Fe-S Cluster

truncations in the NTD region of human mtDNA helicase reduce both helicase activity and the processivity of the mitochondrial DNA replisome (33). This suggests that the NTD plays a vital role in mtDNA metabolism and that this role may have been either retained or obtained within the course of evolution. Our analysis of the NTD from *Drosophila* presents evidence that a metazoan mtDNA helicase has retained the modular architecture inherent to bacterial DnaG-like and T-odd phage primases. The NTD in T7 gp4 binds zinc within a highly conserved stretch of four cysteine residues in the ZBD. Remarkably these four cysteines are strictly conserved in insects and not in vertebrate metazoans (21, 36).

We provide evidence that the NTD of *D. melanogaster* mtDNA helicase does not bind zinc but instead coordinates an iron-sulfur cluster where zinc is bound in T7 gp4. Its UV-visible spectrum is typical of 2Fe-2S and 4Fe-4S proteins. Iron-sulfur proteins that undergo reversible oxidation-reduction reactions are often sensitive to an excess of reductant, although this is not always the case, depending on the function and accessibility of the Fe-S cluster. The addition of dithionite, for example, leads to a decrease in the absorbance peak at 419 nm in the LH28-DA154 protein, and subsequent reoxidation upon exposure to air reverses the effect (37). The apparent insensitivity of the NTD to the presence of reactive oxygen species, and to the presence of various reducing and oxidizing agents is observed in other Fe-S proteins (38–42). In such cases, the function of the cluster may differ from the typical electron transfer function of Fe-S proteins such as those in the mitochondrial electron transport chain and indeed, it has been documented that Fe-S proteins can have other sensing and regulatory functions that do not require their ability to be reversibly reduced (43). They can also act as stabilizing agents for proteins, as well as possess the ability to stabilize specific structures (44). Both elemental analysis and mass spectrometric data suggest that a cluster larger than a 2Fe-2S is unlikely, and thus at present, we conclude that the iron-sulfur cluster in the NTD is a 2Fe-2S center. Whether or not this is the physiological form remains to be determined. The transformation of motif I within the ZBD from zinc to iron-sulfur binding is, to our knowledge, the first to be reported in the evolution of an enzyme. At the same time, human mtDNA helicase lacks the conserved cysteine residues, and we have no data suggesting that it coordinates metal ions. Thus, the evolutionary switch from binding zinc to iron, to loss of metal binding is of substantial interest, and warrants future investigation.

Until recently, the association of a protein with an iron-sulfur cluster was restricted largely to respiratory chain proteins and other regulatory redox enzymes, and not to nucleic acid-binding proteins (45). Nevertheless, iron-sulfur clusters have now been identified in a number of enzymes of nucleic acid metabolism (46), including super family 2 DNA helicases (e.g. XPD, FancJ, RTEL, and DinG) (47, 48). These clusters have been proposed to serve a variety of roles from strictly structural, to redox sensing, to DNA binding and lesion detection (46). Recently, it was reported that the FancJ helicase (and not the related XPD or DDX11) is responsible for unwinding of G4 quadruplex DNA, and thus contributing to genomic stability. This function appears to be unique among Fe-S-containing helicases (49).

The role of iron-sulfur clusters in eukaryotic DNA polymerases is also of substantial interest. Yeast DNA polymerases require the coordination of an iron-sulfur cluster to form active complexes, and thus the integrity of the nuclear genome is dependent on the cluster (50).

The presence of the iron-sulfur cluster in the NTD of *D. melanogaster* mtDNA helicase enhances the stability of the protein *in vitro*. We suggest that the cluster may also regulate its biological functions *in vivo*. For example, during oxidative stress, an iron-sulfur cluster is particularly labile to damage. A damaged iron-sulfur center in the accessory subunit of yeast DNA polymerase leads to the attenuation of DNA replication due to its gradual dissociation from the catalytic subunit (50). A similar outcome may be extrapolated to a replicative DNA helicase, in which a damaged iron-sulfur cluster may lead to protein instability that results in stalling of the replication machinery.

The purified *Drosophila* NTD binds DNA with low affinity as compared with the full-length human mtDNA helicase (32). A DNA-binding function in the NTD is perhaps not surprising considering its substantial sequence homology with T7 gp4, which binds nucleotides and DNA in its DNA primase capacity. In T7 primase, the affinity for hexanucleotide DNA is weak, and binding affinity increases with increasing oligomer size (51, 52). Although the NTD in metazoan mtDNA helicase does not possess primase activity, we report that the *Drosophila* NTD binds both single- and double-stranded oligonucleotides with similar affinities. We postulate that it may serve a role to access DNA at the replication fork by binding it transiently to facilitate delivery to the helicase domain within the mtDNA replisome.

*Acknowledgments*—We express our gratitude to Prof. A. Daniel Jones and the staff in the Mass Spectrometry Facility at Michigan State University for experimental support and many useful discussions. We thank Drs. Lisa Lapidus, Eric Hegg, and Kathryn Severin for access to various instruments. We thank Dr. Magdalena Makowska for early work on the purification and characterization of the NTD protein, and Trisha Cooper for help in the production of the NTD variants.

## REFERENCES

1. Andrews, R. M., Kubacka, I., Chinnery, P. F., Lightowlers, R. N., Turnbull, D. M., and Howell, N. (1999) Reanalysis and revision of the Cambridge reference sequence for human mitochondrial DNA. *Nat. Genet.* **23**, 147
2. Chinnery, P. F., and Hudson, G. (2013) Mitochondrial genetics. *Br. Med. Bull.* **106**, 135–159
3. El-Hattab, A. W., and Scaglia, F. (2013) Mitochondrial DNA depletion syndromes: review and updates of genetic basis, manifestations, and therapeutic options. *Neurotherapeutics* **10**, 186–198
4. Copeland, W. C. (2012) Defects in mitochondrial DNA replication and human disease. *Crit. Rev. Biochem. Mol. Biol.* **47**, 64–74
5. Korhonen, J. A., Pham, X. H., Pellegrini, M., and Falkenberg, M. (2004) Reconstitution of a minimal mtDNA replisome *in vitro*. *EMBO J.* **23**, 2423–2429
6. Korhonen, J. A., Gaspari, M., and Falkenberg, M. (2003) TWINKLE Has 5' → 3' DNA helicase activity and is specifically stimulated by mitochondrial single-stranded DNA-binding protein. *J. Biol. Chem.* **278**, 48627–48632
7. Spelbrink, J. N., Li, F. Y., Tiranti, V., Nikali, K., Yuan, Q. P., Tariq, M., Wanrooij, S., Garrido, N., Comi, G., Morandi, L., Santoro, L., Toscano, A., Fabrizi, G. M., Somer, H., Croxen, R., Beeson, D., Poulton, J., Suomalainen, A., Jacobs, H. T., Zeviani, M., and Larsson, C. (2001) Human mitochondrial DNA deletions associated with mutations in the gene encoding Twinkle, a phage T7 gene 4-like protein localized in mitochondria. *Nat.*

- Genet.* **28**, 223–231
8. Suhasini, A. N., and Brosh, R. M., Jr. (2013) Disease-causing missense mutations in human DNA helicase disorders. *Mutat. Res.* **752**, 138–152
  9. Matsushima, Y., and Kaguni, L. S. (2007) Differential phenotypes of active site and human autosomal dominant progressive external ophthalmoplegia mutations in *Drosophila* mitochondrial DNA helicase expressed in Schneider cells. *J. Biol. Chem.* **282**, 9436–9444
  10. Matsushima, Y., and Kaguni, L. S. (2009) Functional importance of the conserved N-terminal domain of the mitochondrial replicative DNA helicase. *Biochim. Biophys. Acta* **1787**, 290–295
  11. Sanchez-Martinez, A., Calleja, M., Peralta, S., Matsushima, Y., Hernandez-Sierra, R., Whitworth, A. J., Kaguni, L. S., and Garesse, R. (2012) Modeling pathogenic mutations of human Twinkle in *Drosophila* suggests an apoptosis role in response to mitochondrial defects. *PLoS One* **7**, e43954
  12. Wanrooij, S., and Falkenberg, M. (2010) The human mitochondrial replication fork in health and disease. *Biochim. Biophys. Acta* **1797**, 1378–1388
  13. Tynynmaa, H., Sembongi, H., Bokori-Brown, M., Granycome, C., Ashley, N., Poulton, J., Jalanko, A., Spelbrink, J. N., Holt, I. J., and Suomalainen, A. (2004) Twinkle helicase is essential for mtDNA maintenance and regulates mtDNA copy number. *Hum. Mol. Genet.* **13**, 3219–3227
  14. Ziebarth, T. D., Farr, C. L., and Kaguni, L. S. (2007) Modular architecture of the hexameric human mitochondrial DNA helicase. *J. Mol. Biol.* **367**, 1382–1391
  15. Ziebarth, T. D., Gonzalez-Soltero, R., Makowska-Grzyska, M. M., Núñez-Ramírez, R., Carazo, J. M., and Kaguni, L. S. (2010) Dynamic effects of cofactors and DNA on the oligomeric state of human mitochondrial DNA helicase. *J. Biol. Chem.* **285**, 14639–14647
  16. Makowska-Grzyska, M. M., Ziebarth, T. D., and Kaguni, L. S. (2010) Physical analysis of recombinant forms of the human mitochondrial DNA helicase. *Methods* **51**, 411–415
  17. Toth, E. A., Li, Y., Sawaya, M. R., Cheng, Y., and Ellenberger, T. (2003) The crystal structure of the bifunctional primase-helicase of bacteriophage T7. *Mol. Cell* **12**, 1113–1123
  18. Bird, L. E., Håkansson, K., Pan, H., and Wigley, D. B. (1997) Characterization and crystallization of the helicase domain of bacteriophage T7 gene 4 protein. *Nucleic Acids Res.* **25**, 2620–2626
  19. Patel, S. S., and Picha, K. M. (2000) Structure and function of hexameric helicases. *Annu. Rev. Biochem.* **69**, 651–697
  20. Guo, S., Tabor, S., and Richardson, C. C. (1999) The linker region between the helicase and primase domains of the bacteriophage T7 gene 4 protein is critical for hexamer formation. *J. Biol. Chem.* **274**, 30303–30309
  21. Shutt, T. E., and Gray, M. W. (2006) Twinkle, the mitochondrial replicative DNA helicase, is widespread in the eukaryotic radiation and may also be the mitochondrial DNA primase in most eukaryotes. *J. Mol. Evol.* **62**, 588–599
  22. Kusakabe, T., Hine, A. V., Hyberts, S. G., and Richardson, C. C. (1999) The Cys4 zinc finger of bacteriophage T7 primase in sequence-specific single-stranded DNA recognition. *Proc. Natl. Acad. Sci. U.S.A.* **96**, 4295–4300
  23. Frick, D. N., Baradaran, K., and Richardson, C. C. (1998) An N-terminal fragment of the gene 4 helicase/primase of bacteriophage T7 retains primase activity in the absence of helicase activity. *Proc. Natl. Acad. Sci. U.S.A.* **95**, 7957–7962
  24. Gasteiger E. H. C., Gattiker, A., Duvaud, S., Wilkins, M. R., Appel, R. D., and Bairoch, A. (2005) Protein identification and analysis tools on the ExpASY server. In *The Proteomics Identification Handbook* (Walker, J. M., ed) pp. 38, Humana Press, Totowa, NJ
  25. Huang, Q., Hong, X., and Hao, Q. (2008) SNAP-25 is also an iron-sulfur protein. *FEBS Lett.* **582**, 1431–1436
  26. Chen, D., and Frey, P. A. (2001) Identification of lysine 346 as a functionally important residue for pyridoxal 5′-phosphate binding and catalysis in lysine 2,3-aminomutase from *Bacillus subtilis*. *Biochemistry* **40**, 596–602
  27. Rabinowitz, J. C. (1978) Analysis of acid-labile sulfide and sulfhydryl groups. *Methods Enzymol.* **53**, 275–277
  28. Whitmore, L., and Wallace, B. A. (2004) DICHROWEB, an online server for protein secondary structure analyses from circular dichroism spectroscopic data. *Nucleic Acids Res.* **32**, W668–W673
  29. Whitmore, L., and Wallace, B. A. (2008) Protein secondary structure analyses from circular dichroism spectroscopy: methods and reference data-bases. *Biopolymers* **89**, 392–400
  30. Kelley, L. A., and Sternberg, M. J. (2009) Protein structure prediction on the Web: a case study using the Phyre server. *Nat. Protoc.* **4**, 363–371
  31. Pugh, R. A., Honda, M., and Spies, M. (2010) Ensemble and single-molecule fluorescence-based assays to monitor DNA binding, translocation, and unwinding by iron-sulfur cluster containing helicases. *Methods* **51**, 313–321
  32. Longley, M. J., Humble, M. M., Sharief, F. S., and Copeland, W. C. (2010) Disease variants of the human mitochondrial DNA helicase encoded by C10orf2 differentially alter protein stability, nucleotide hydrolysis, and helicase activity. *J. Biol. Chem.* **285**, 29690–29702
  33. Farge, G., Holmlund, T., Khvorostova, J., Rofougaran, R., Hofer, A., and Falkenberg, M. (2008) The N-terminal domain of TWINKLE contributes to single-stranded DNA binding and DNA helicase activities. *Nucleic Acids Res.* **36**, 393–403
  34. Holmlund, T., Farge, G., Pande, V., Korhonen, J., Nilsson, L., and Falkenberg, M. (2009) Structure-function defects of the twinkle amino-terminal region in progressive external ophthalmoplegia. *Biochim. Biophys. Acta* **1792**, 132–139
  35. Goffart, S., Cooper, H. M., Tynynmaa, H., Wanrooij, S., Suomalainen, A., and Spelbrink, J. N. (2009) Twinkle mutations associated with autosomal dominant progressive external ophthalmoplegia lead to impaired helicase function and *in vivo* mtDNA replication stalling. *Hum. Mol. Genet.* **18**, 328–340
  36. Ilyina, T. V., and Koonin, E. V. (1992) Conserved sequence motifs in the initiator proteins for rolling circle DNA replication encoded by diverse replicons from eubacteria, eucaryotes and archaeobacteria. *Nucleic Acids Res.* **20**, 3279–3285
  37. Khoroshilova, N., Beinert, H., and Kiley, P. J. (1995) Association of a polynuclear iron-sulfur center with a mutant FNR protein enhances DNA binding. *Proc. Natl. Acad. Sci. U.S.A.* **92**, 2499–2503
  38. Ding, H., and Dimple, B. (1998) Thiol-mediated disassembly and reassembly of [2Fe-2S] clusters in the redox-regulated transcription factor SoxR. *Biochemistry* **37**, 17280–17286
  39. Reents, H., Gruner, I., Harmening, U., Böttger, L. H., Layer, G., Heathcote, P., Trautwein, A. X., Jahn, D., and Härtig, E. (2006) *Bacillus subtilis* Fnr senses oxygen via a [4Fe-4S] cluster coordinated by three cysteine residues without change in the oligomeric state. *Mol. Microbiol.* **60**, 1432–1445
  40. Lillig, C. H., Berndt, C., Vergnolle, O., Lönn, M. E., Hudemann, C., Bill, E., and Holmgren, A. (2005) Characterization of human glutaredoxin 2 as iron-sulfur protein: a possible role as redox sensor. *Proc. Natl. Acad. Sci. U.S.A.* **102**, 8168–8173
  41. Singh, A., Guidry, L., Narasimhulu, K. V., Mai, D., Trombley, J., Redding, K. E., Giles, G. I., Lancaster, J. R., Jr., and Steyn, A. J. (2007) *Mycobacterium tuberculosis* WhiB3 responds to O<sub>2</sub> and nitric oxide via its [4Fe-4S] cluster and is essential for nutrient starvation survival. *Proc. Natl. Acad. Sci. U.S.A.* **104**, 11562–11567
  42. Jervis, A. J., Crack, J. C., White, G., Artymiuk, P. J., Cheesman, M. R., Thomson, A. J., Le Brun, N. E., and Green, J. (2009) The O<sub>2</sub> sensitivity of the transcription factor FNR is controlled by Ser24 modulating the kinetics of [4Fe-4S] to [2Fe-2S] conversion. *Proc. Natl. Acad. Sci. U.S.A.* **106**, 4659–4664
  43. Beinert, H., Holm, R. H., and Münck, E. (1997) Iron-sulfur clusters: nature's modular, multipurpose structures. *Science* **277**, 653–659
  44. Beinert, H., Meyer, J., and Lill, R. (2004) Iron-sulfur proteins. In *Encyclopedia of Biological Chemistry* (Lennarz, W. J., and Lane, M. D., eds) pp. 482–489, Elsevier, New York
  45. Ferrer, M., Golyshina, O. V., Beloqui, A., Golyshin, P. N., and Timmis, K. N. (2007) The cellular machinery of *Ferroplasma acidiphilum* is iron-protein-dominated. *Nature* **445**, 91–94
  46. White, M. F., and Dillingham, M. S. (2012) Iron-sulphur clusters in nucleic acid processing enzymes. *Curr. Opin. Struct. Biol.* **22**, 94–100
  47. Rudolf, J., Makrantonis, V., Ingledew, W. J., Stark, M. J., and White, M. F. (2006) The DNA repair helicases XPD and FancJ have essential iron-sulfur domains. *Mol. Cell* **23**, 801–808
  48. White, M. F. (2009) Structure, function and evolution of the XPD family of iron-sulfur-containing 5′ → 3′ DNA helicases. *Biochem. Soc. Trans.* **37**, 547–551

## ***Dm mtDNA Helicase Contains an Fe-S Cluster***

49. Bharti, S. K., Sommers, J. A., George, F., Kuper, J., Hamon, F., Shin-ya, K., Teulade-Fichou, M. P., Kisker, C., and Brosh, R. M., Jr. (2013) Specialization among iron-sulfur cluster helicases to resolve G-quadruplex DNA structures that threaten genomic stability. *J. Biol. Chem.* **288**, 28217–28229
50. Netz, D. J., Stith, C. M., Stümpfig, M., Köpf, G., Vogel, D., Genau, H. M., Stodola, J. L., Lill, R., Burgers, P. M., and Pierik, A. J. (2012) Eukaryotic DNA polymerases require an iron-sulfur cluster for the formation of active complexes. *Nat. Chem. Biol.* **8**, 125–132
51. Frick, D. N., and Richardson, C. C. (1999) Interaction of bacteriophage T7 gene 4 primase with its template recognition site. *J. Biol. Chem.* **274**, 35889–35898
52. Lee, S. J., Zhu, B., Hamdan, S. M., and Richardson, C. C. (2010) Mechanism of sequence-specific template binding by the DNA primase of bacteriophage T7. *Nucleic Acids Res.* **38**, 4372–4383

## The N-terminal Domain of the *Drosophila* Mitochondrial Replicative DNA Helicase Contains an Iron-Sulfur Cluster and Binds DNA

Johnny Stiban, Gregory A. Farnum, Stacy L. Hovde and Laurie S. Kaguni

*J. Biol. Chem.* 2014, 289:24032-24042.

doi: 10.1074/jbc.M114.587774 originally published online July 14, 2014

---

Access the most updated version of this article at doi: [10.1074/jbc.M114.587774](https://doi.org/10.1074/jbc.M114.587774)

### Alerts:

- [When this article is cited](#)
- [When a correction for this article is posted](#)

[Click here](#) to choose from all of JBC's e-mail alerts

This article cites 50 references, 23 of which can be accessed free at <http://www.jbc.org/content/289/35/24032.full.html#ref-list-1>